Journal of Science and Technology in Civil Engineering, HUCE (NUCE), 2022, 16 (1): 138–151

EFFECT OF PRE-TENSIONED ROPE TENSIONS ON A LADDER STRUCTURE OF TURNTABLE LADDERS

Van Tinh Nguyen[a,*]

[a]*Faculty of Mechanical Engineering, Hanoi University of Civil Engineering, 55 Giai Phong road, Hai Ba Trung district, Hanoi, Vietnam*

Article history:
Received 20/8/2021, Revised 28/9/2021, Accepted 01/10/2021

Abstract

To expand the operating zone and control more precisely, it is vital to enhance the flexural stiffness of the ladder structures of turntable ladders. Based on one set of optimized 3-segment ladders, the author proposed a solution to increase the bending stiffness on each ladder while their mass hardly increases. Steel wire ropes are suggested to be added inside the handrails. They are pre-stretched and controlled to reduce the vertical displacement and rapidly quench oscillation at the ladder top. These benefits have been demonstrated in the dynamic aspect in other works. In this study, the effect of pre-tensioned rope tensions on ladder structure is investigated and evaluated according to current standards. The work includes modeling the ladder structure, defining loads, combining loads, investigating stresses and displacements according to the tension values. Afterward, the positive effects and negative influences, as well as the recommendations on tension load and tensile process, are presented. According to the obtained results, the structure still ensures the working conditions while the tension value reaches the maximum one. Most of the stress values in the structural elements decrease with increasing tension. The vertical displacement at the top decreases significantly.

Keywords: turntable ladder; ladder structure; load combination; pre-tensioned rope tension; flexural stiffness.

https://doi.org/10.31814/stce.huce(nuce)2022-16(1)-12

1. Introduction

Rescues in high-rise buildings are of particular interest because of their complexity, danger, and a terrible level of destruction if an incident such as fire, explosion, or terrorism occurs. Solutions include on-site rescues and outside rescues (mainly from professional rescuers). Corresponding to them is the research and development of rescue equipment for these two solution groups. In the first group, the objects studied are as diverse as the built-in rescue equipment in the building [1], the personal rescue winch [2], and the individual rescue winch combined with one guide ladder set and one rescue cage for serving to various victims [3, 4]. Meanwhile, turntable ladders are common equipment for rescue used by professional rescuers. Today, they are indispensable equipment for this work because of their mobility, fast rescue speed, and outstanding features when combined with other equipment. The general structure of a typical turntable ladder is shown in Fig. 1(a). Its main divisions include 1 - Truck, 2 - Turntable, 3 - Luffing cylinder, 4 - Ladder section 3, 5 - Ladder section 2, 6 - Ladder section 1 and 7 - Rescue cage. Its ladder structure has the form described in [5]. The luffing cylinder carries out the lifting and lowering. The ladder extension is carried out by hydraulic cylinder 8, retracted rope

*Corresponding author. *E-mail address:* tinhnv@nuce.edu.vn (Nguyen, V. T.)

9 and extended rope 10 linked together according to the rope diagram in Fig. 1(b) [6]. The studies related to turntable ladders are mainly aimed at increasing their working ability, such as the vibration damping control for a ladder with a length of more than 50 m [7, 8], the active vibration damping control for one boom of articulated aerial ladders [9], and increased flexural stiffness combined with vibration reduction control through the control of the additional steel ropes in the handrails [10, 11]. In two studies later, the effect of reducing static displacement and rapidly quenching vibration is discovered in the dynamic aspect. However, the impact of the added steel tensions on the ladder structure has not been investigated and evaluated exhaustively. Therefore, this study aims to address this outstanding work.

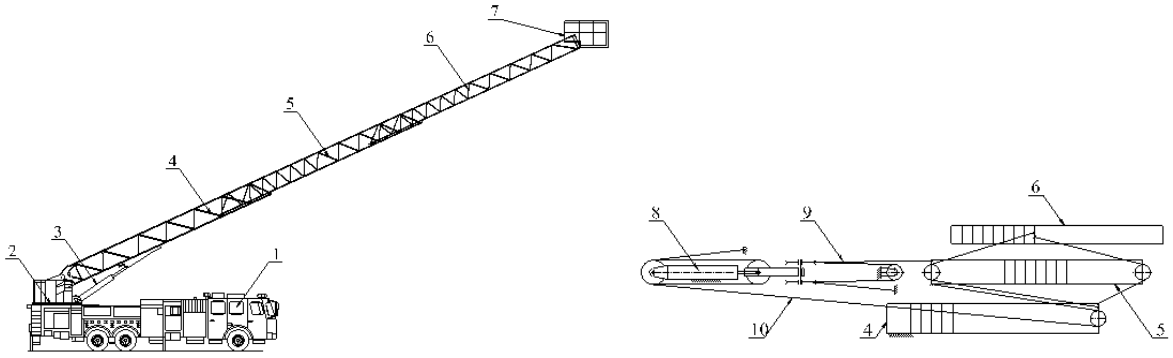

(a) (b)

Figure 1. A typical turntable ladder (a) and the telescoping rope diagram (b)

The testing and evaluation of the working ability of truss structures have also been presented in various literature, such as calculating the tower crane structure [12] and formwork structure [13]. However, due to different working conditions and working principle characteristics, they cannot be applied to the work for the turntable ladders. Furthermore, the applicable standards are also different. The structure and working characteristics of the ladder set described in the solution of [10, 11] are different from that of conventional turntable ladders. The calculation here should be carried out according to safety standards with various loads and a variety of different states, so the work is also different from the swing investigation of an aerial ladder caused by sudden wind loads in [14].

Based on the structure of one existing ladder, the work in this study includes modeling it, determining the loads and load combinations, and checking the working ability of the structure according to relevant standards. Afterward, the author investigates and evaluates the effect of the added steel ropes on the ladder structure. Recommendations and recommendations for the rope tension loads, tensioning process, and effective performance conditions. The structural calculation method applied in the study is the finite element method, which is the foundational calculation method in common structural calculation programs.

2. Ladder configuration, assumptions, and boundary conditions

2.1. Ladder configuration

All geometric parameters of the ladder used for modeling and analyzing the structure are taken from the patent application publication US 2009/0101436 A1. The truss ladder depicted in [5] consists of three ladder sections. The maximum work height counted from the ground to the handrail of the

cage is 30.48 m. It corresponds to the maximum elevation angle in the vertical plane. The lengths of the 1st to 3rd ladder section are 10.9 m, 10.5 m, and 10.5 m, respectively.

The first ladder section is composed of two handrails (□1.5×2/0.305), two rails which have a cross section shown in Fig. 51A in [5], the diagonal members between the handrail and the rail (□1.5×1.25/0.125×0.1 and □1.5×1.5/0.25), the ladder rungs (□2.25×1.45/0.265) and K-braces (□2 ×1.45/0.25). The cross section of the rungs and K-braces is the same in all ladder sections.

The second ladder section comprises two handrails (□2×3/0.5), two rails which have a cross section shown in Fig. 31A in [5] and the diagonal members (□2×2/0.375, □1.75×2/0.12×0.31 and □2.5×2/0.45). The dimensions of the cross sections are expressed in inches.

The third ladder section contains two handrails (□2.25×4/0.6), two rails which have a cross section shown in Fig. 8A in [5], the diagonal members (□2.25×4/0.6, □2×3/0.435, □2×1.75/0.365 and □2×2/0.375) and some plate of 30 mm.

The ladder material is aluminum alloy 6061-T6511 for extruded tubular members and aluminum alloy 6061-T6 for plate members.

2.2. Assumptions

The gravity load of the ladder is the total gravity load of all elements manufactured by aluminum alloy. The gravity loads of the wire ropes, the sheaves, the small electrical and hydraulic equipment, the coating paint, and welds in the ladder are ignored. The tension loads caused by the wire ropes are substituted by single forces placed at the points that the ropes associated with the structure. The wind load is distributed loads. Its value is the greatest value that the machine is still allowed to operate. In the normal environment condition, the load caused by the change of the temperature is trivial. The ladder set is connected to the truck by four hinge joints. The joints are assumed to be absolutely hard.

2.3. Boundary conditions

The calculation, comparison, and evaluation are effectuated at two positions of the elevation angle in the vertical plane as 0° and 75°. Normally, calculating and designing one boom of mobile cranes shall be checked at various positions of the angle. However, for turntable ladders having a constant rated load on the entire elevation angle, the checking is done at the two positions is sufficient.

All loads are considered in terms of what is the most detrimental to the ladder structure. The ladder is in the maximum expansion state. It is the state that the maximum stress can be found out.

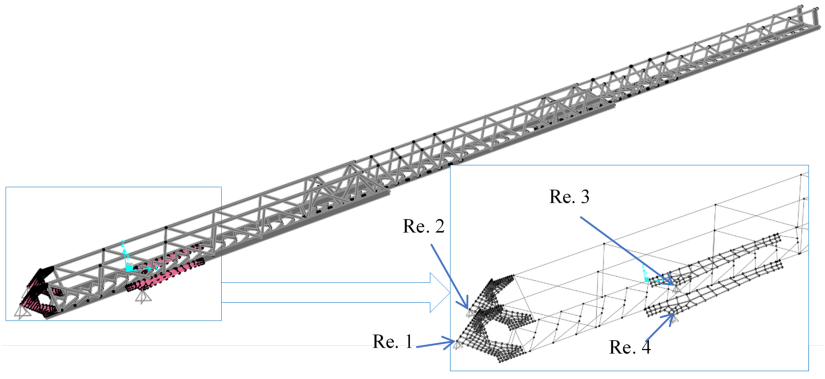

Figure 2. A structural calculation model of the ladder set

The calculation model of the ladder can be modelled as shown in Fig. 2. In which it has had no accompanying loads yet. The restraints between the ladder and the foundation are four joints. Two joints are at the bottom, and the remaining points are at the link positions between the ladder and the hydraulic cylinders. Each joint allows the ladder can rotate freely around it in three directions.

3. Loads and load combinations

3.1. Calculation load

a. Self-weight G

Self-weight G includes the gravity load of the ladder structure G_l and the rescue cage G_c. With the cage dimensions of 1.5 m × 0.83 m × 1.15 m (length × width × height), the weight is replaced by two forces and two moments. They are placed on the rail top of ladder section 1.

b. Rated load Q

The rated load is the maximum load of carried persons, materials, and equipment that the machine can lift. It depends on the working feature of the turntable ladder. The person weight Q_p of 4500 N is equivalent to 5 persons [15]. Its set point is at the center of the cage.

The weight of materials and equipment is an evenly distributed load on 25% of the cage floor as shown in Fig. 3 with two areas of distribution A and B [15]. Applying area A or B relies on the specific load combination to create the maximum stress in the structure. The total distributed load on A is named Q_a and another is Q_b. Total value of the distributed load is 1500 N.

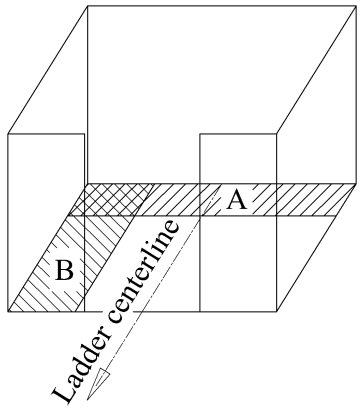

Figure 3. Distributed load areas on the cage floor

c. The forces caused by the telescoping wire ropes F_t

The forces are generated by the tension loads during extending process. Ignoring friction, the forces balance the loads which are created from G and Q in the tilt of the ladder. They are illustrated in Fig. 4. Ignoring the effect of the ladder deformation, the inclination angles at different computational locations are the same φ. Hence, F_{ti} $(i = 1, 2, 3)$ can be calculated in each section as in Eqs. (1)–(6).

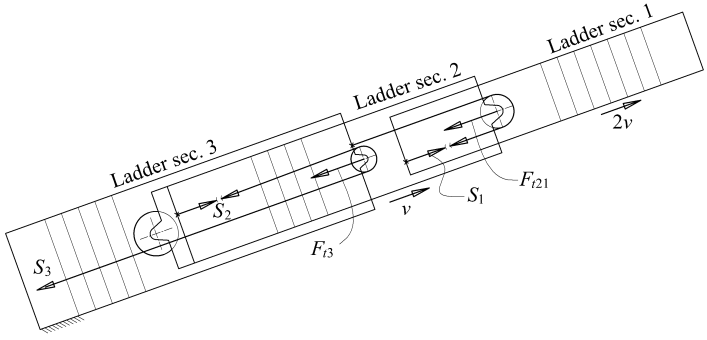

Figure 4. Forces caused by the telescoping wire ropes

In ladder section 1:

$$F_{t1} = S_1 \tag{1}$$

$$S_1 = (G_{l1} + G_c + Q)\sin\varphi \tag{2}$$

where S_1 is the tension of the extend rope in section 1 and G_{l1} is the weight of section 1.

In ladder section 2, F_{t2} includes F_{t21} and F_{t22} at the top and bottom, respectively. They are defined as follows:

$$F_{t21} = 2S_1 \tag{3}$$

$$F_{t22} = S_2 \tag{4}$$

$$S_2 = (G_{l1} + G_{l2} + G_c + Q)\sin\varphi + S_1 \tag{5}$$

where S_2 is the tension of the extend rope in section 2 and G_{l2} is the weight of section 2.

In ladder section 3:

$$F_{t3} = 2S_2 - S_1 \tag{6}$$

d. The forces caused by the added wire ropes F_r

F_r consists of F_{r1}, F_{r2}, and F_{r3} in ladder sections 1, 2, and 3, respectively. These concentrated loads are pre-tension loads of the ropes and are placed at two ends of each handrail. The values of these forces should be set at different values during the calculation. Fig. 5 shows the sense and placed point of the forces. To create different values of each force F_{ri} $(i = 1, 2, 3)$, one adjustment coefficient k_{ri} $(i = 1, 2, 3)$ is multiplied by the initial base value. Based on the maximum tension forces and the limited compressive force of the handrails, the value levels of F_{ri} are proposed as shown in Table 1.

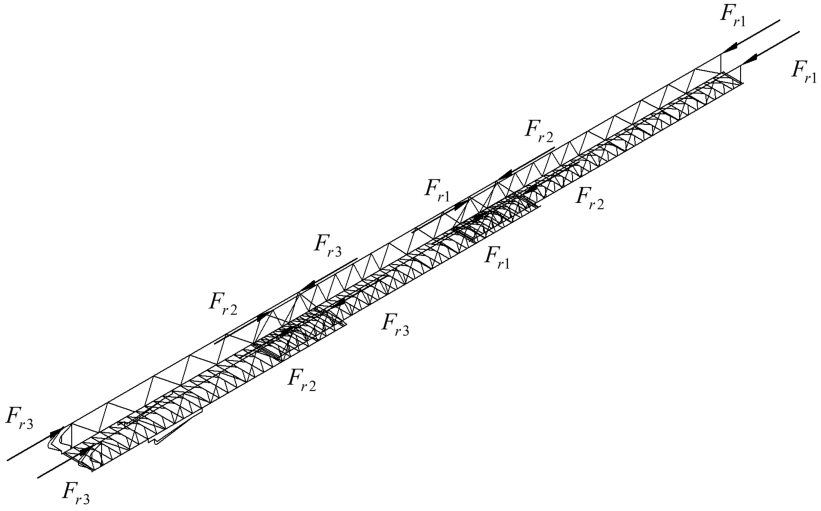

Figure 5. Illustrating the tensions of the wire ropes

e. The loads caused by the acceleration of the telescoping drive F_{at}

The telescoping drive creates the extending/retracting motion of the ladder set. It is assumed that the rescue cage reaches a telescoping velocity of 2 m/s in an acceleration time of 4 s. Hence, the telescoping acceleration of the 1st section is $a_1 = 0.5$ m/s^2 and of the 2nd section is $a_2 = 0.25$ m/s^2.

Table 1. The values of F_{ri} ($i = 1 - 3$) corresponding to the adjustment coefficient

Level	1	2	3	4	5	6	7	8
k_{ri}	0	0.5	1	2	3	4	5	6
F_{r1} (N)	0	250	500	1000	1500	2000	2500	3000
F_{r2} (N)	0	1250	2500	5000	7500	10000	12500	15000
F_{r3} (N)	0	2500	5000	10000	15000	20000	25000	30000

f. The loads caused by the acceleration of the slewing drive F_s

According to [16], an angular acceleration can be chosen of 0.013 rad/s^2. The value corresponds to the acceleration of 0.4 m/s^2 at the ladder top and an acceleration time of 5.25 s (the angular velocity value varies between 0 and 0.07 rad/s). The loads caused by the acceleration of the slewing drive include an inertia force F_{s1} and a centrifugal force F_{s2}. For simplicity of calculation, at the frame elements the loads are ignored because they are small and differently distributed in the elements.

g. The loads caused by the acceleration of the luffing drive F_l

The luffing motion in a mobile crane is the lowering/raising motion in a turntable ladder [17]. With the elevation angle velocity value equivalent to the slewing angle velocity value, the inertia force F_{l1} and the centrifugal force F_{l2} are similarly calculated. The value of r_i is replaced by corresponding values, respectively.

h. Wind load F_w

Because the turntable ladder only works in case of need, the wind load is only considered during the work. It can be called the wind load in the working state F_w. The wind direction is assumed to be horizontal, and the wind pressure does not change with height. The load affects the ladder truss structure, the cage and the persons standing in the cage. Its maximum value which the vehicle can still work is limited by a safe equipment usually mounting on the ladder top or on the cage.

The wind load should be calculated in three cases. The first one is when the wind load perpendicular the vertical plane containing the ladder. The second one is in the vertical plane containing the ladder with the wind direction from rear to front. The last case is in the vertical plane containing the ladder with the wind direction from front to rear.

According to [16], the wind load part impacting on the cage and the persons is defined (in N) as follows:

$$F_{w1} = A_w \cdot q_w \cdot c_f \tag{7}$$

where A_w is the effective frontal area, m^2; q_w is the wind pressure, $q_w = 100$ N/m^2 corresponding to the wind speed of 12.5 m/s (Beaufort Scale 6) [15]; c_f is the shape coefficient of the consideration element in the direction of the wind.

The persons standing in the cage are partially obscured by its structure and rescue devices. To simplify the calculation, here, the wind contact surface of the cage is assumed to be a large flat area. Therefore, its front exposed area is 1.725 m^2 and its side exposed area is 0.955 m^2. The exposed area of one person should be 0.35 m^2 [18]. With five persons including three persons standing in front and two persons standing behind, when calculating the wind load impacting on two behind standing persons, a shielding factor c_η is multiplied into Eq. (7).

The wind load parts impacting the cage and the persons are considered two single forces and transformed into the equivalent loads placed on the ladder top.

The wind load part impacting on the frame elements of the ladder structure is defined in N/m as follows:

$$F_{w2} = \frac{A_w \cdot q_w \cdot c_f}{l_w} \tag{8}$$

with l_w is the length of the frame element in the calculation plane, m.

For the windward frame or member and the unsheltered parts of those behind it, the value of the shape coefficient corresponding to each element is listed in Table 2.

Table 2. Values of the shape coefficient

Type	Main rail of the 1st ladder section	Main rail of the 2nd ladder section	Main rail of the 3rd ladder section	Box sections	Large flat areas	Person directly exposed
c_f	1.6	1.6	1.4	1.4	1.2	1

For the sheltered parts, the wind load is also calculated as in Eq. (7) and Eq. (8) and is multiplied by c_η. Based on the parameters of each ladder section, the factor will be determined through the solidity ration and spacing ratio. The solidity and spacing rations of all sections are chosen following [18, 19] and shown in Table 3.

Table 3. Values of the shielding factor

Type	1st lad. section	2nd lad. section	3rd lad. section	Person
Solidity ration	2.9/7.19	3.56/7.88	4/9.03	-
Spacing ration	784.2/660.9	990.6/753.6	1206.5/863.6	-
c_η	0.43	0.43	0.43	0.6

i. Manual force F_m

The value of the force is 400 N acting at a height of 1.1 m above the cage floor [15]. In the calculation, the force direction is the most unfavourable direction for the structure. Hence, the force is placed at the farthest corner of the cage and its direction is set as in the following cases: perpendicular to the vertical plane containing the ladder F_{mh}; in the side plane of the cage, perpendicular to the ladder and downward F_{md}; and like the previous one but upward F_{mu}. They are Illustrated as in Fig. 6.

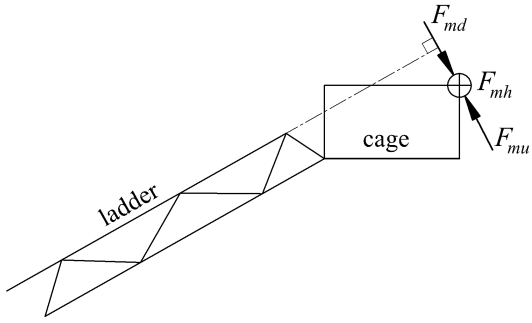

Figure 6. Illustrating for the different calculation cases of the manual force

3.2. Load combination

The load combination must be considered in three calculation cases as the machine works without in-service wind, with in-service wind, and under test conditions. The first case consists of nine load combinations, as listed in Table 4. The working states of the ladder include telescoping at the special

location and moving with combinations (telescoping + luffing) and (telescoping + slewing) at $\varphi = 0^\circ$ and $\varphi = 75^\circ$.

Table 4. Load combinations in the first case

No.	Combination	Load combination formula	$\varphi(^\circ)$		Factor value [20, 21]
			0	75	
1	Comb. 1	$\beta\left[\beta_1 \cdot G + \beta_2 (F_r + F_t)\right]$		×	
2	Comb. 2	$\beta\left[\beta_1 \cdot G + \beta_2 \left(Q_p + Q_a + F_{md} + F_r + F_t\right)\right]$	×		
3	Comb. 3	$\beta\left[\beta_1 \cdot G + \beta_2 \left(Q_p + Q_a + F_{mu} + F_r + F_t\right)\right]$		×	
4	Comb. 4	$\beta\left[\beta_1 \cdot G + \beta_2 \left(Q_p + Q_b + F_{md} + F_r + F_t\right)\right]$	×		$\beta = 1.48$
5	Comb. 5	$\beta\left[\beta_1 \cdot G + \beta_2 \left(Q_p + Q_b + F_{mu} + F_r + F_t\right)\right]$		×	$\beta_1 = 1$ $\beta_2 = 1$ $\beta_3 = 1.2$
6	Comb. 6	$\beta\left[\beta_1 \cdot G + \beta_2 \left(Q_p + Q_a + F_r + F_t\right) + \beta_3 (F_{at} + F_l)\right]$	×	×	
7	Comb. 7	$\beta\left[\beta_1 \cdot G + \beta_2 \left(Q_p + Q_b + F_r + F_t\right) + \beta_3 (F_{at} + F_l)\right]$	×	×	
8	Comb. 8	$\beta\left[\beta_1 \cdot G + \beta_2 \left(Q_p + Q_a + F_r + F_t\right) + \beta_3 (F_{at} + F_s)\right]$	×	×	
9	Comb. 9	$\beta\left[\beta_1 \cdot G + \beta_2 \left(Q_p + Q_b + F_r + F_t\right) + \beta_3 (F_{at} + F_s)\right]$	×	×	

The second case consists of eighteen load combinations, as listed in Table 5. The wind direction mentioned is from back to the front of the ladder, from front to the back of the ladder, and perpendicular to the vertical plane containing the ladder.

Table 5. Load combinations in the second case

No.	Combination	Load combination formula	φ (°)		Factor value [20, 21]
			0	75	
1	Comb. 10	$\beta\left[\beta_1 \cdot G + \beta_2 \left(Q_p + Q_a + F_{md} + F_r + F_t\right) + F_{wb}\right]$		×	
2	Comb. 11	$\beta\left[\beta_1 \cdot G + \beta_2 \left(Q_p + Q_b + F_{md} + F_r + F_t\right) + F_{wb}\right]$		×	
3	Comb. 12	$\beta\left[\beta_1 \cdot G + \beta_2 \left(Q_p + Q_a + F_r + F_t\right) + \beta_3 (F_{at} + F_l) + F_{wb}\right]$		×	
4	Comb. 13	$\beta\left[\beta_1 \cdot G + \beta_2 \left(Q_p + Q_b + F_r + F_t\right) + \beta_3 (F_{at} + F_l) + F_{wb}\right]$		×	$\beta = 1.34$
5	Comb. 14	$\beta\left[\beta_1 \cdot G + \beta_2 \left(Q_p + Q_a + F_r + F_t\right) + \beta_3 (F_{at} + F_s) + F_{wb}\right]$		×	$\beta_1 = 1$ $\beta_2 = 1$
6	Comb. 15	$\beta\left[\beta_1 \cdot G + \beta_2 \left(Q_p + Q_b + F_r + F_t\right) + \beta_3 (F_{at} + F_s) + F_{wb}\right]$		×	$\beta_3 = 1$
7	Comb. 16	$\beta\left[\beta_1 \cdot G + \beta_2 (F_r + F_t) + \beta_3 (F_{at} + F_l) + F_{wf}\right]$		×	
8	Comb. 17	$\beta\left[\beta_1 \cdot G + \beta_2 (F_r + F_t) + \beta_3 (F_{at} + F_s) + F_{wf}\right]$		×	
9	Comb. 18	$\beta\left[\beta_1 \cdot G + \beta_2 \left(Q_p + Q_a + F_{mh} + F_r + F_t\right) + F_{wp}\right]$	×	×	
10	Comb. 19	$\beta\left[\beta_1 \cdot G + \beta_2 \left(Q_p + Q_b + F_{mh} + F_r + F_t\right) + F_{wp}\right]$	×	×	

No.	Combination	Load combination formula	φ (°)		Factor value [20, 21]
			0	75	
11	Comb. 20	$\beta\left[\beta_1.G+\beta_2\left(Q_p+Q_a+F_{md}+F_r+F_t\right)+F_{wp}\right]$	×		
12	Comb. 21	$\beta\left[\beta_1\cdot G+\beta_2\left(Q_p+Q_b+F_{md}+F_r+F_t\right)+F_{wp}\right]$	×		
13	Comb. 22	$\beta\left[\beta_1.G+\beta_2\left(Q_p+Q_a+F_{mu}+F_r+F_t\right)+F_{wp}\right]$		×	$\beta = 1.34$
14	Comb. 23	$\beta\left[\beta_1\cdot G+\beta_2\left(Q_p+Q_b+F_{mu}+F_r+F_t\right)+F_{wp}\right]$		×	$\beta_1 = 1$
15	Comb. 24	$\beta\left[\beta_1\cdot G+\beta_2\left(Q_p+Q_a+F_r+F_t\right)+\beta_3\left(F_{at}+F_l\right)+F_{wp}\right]$	×	×	$\beta_2 = 1$ $\beta_3 = 1$
16	Comb. 25	$\beta\left[\beta_1\cdot G+\beta_2\left(Q_p+Q_b+F_r+F_t\right)+\beta_3\left(F_{at}+F_l\right)+F_{wp}\right]$	×	×	
17	Comb. 26	$\beta\left[\beta_1\cdot G+\beta_2\left(Q_p+Q_a+F_r+F_t\right)+\beta_3\left(F_{at}+F_s\right)+F_{wp}\right]$	×	×	
18	Comb. 27	$\beta\left[\beta_1\cdot G+\beta_2\left(Q_p+Q_b+F_r+F_t\right)+\beta_3\left(F_{at}+F_s\right)+F_{wp}\right]$	×	×	

The third case consists of nine load combinations, as listed in Table 6. A test load of 125% of the rated load [22] has the applicable position as in Fig. 7, and the ladder is checked at $\varphi = 0°$ and $\varphi = 75°$ in the static test. The dynamic test is effectuated in the condition having wind and a test load of 110% of the rated load [22].

Two combinations 35 and 36 are performed at the maximum possible elevation angle and the maximum possible extension. They are used to evaluate displacement conditions.

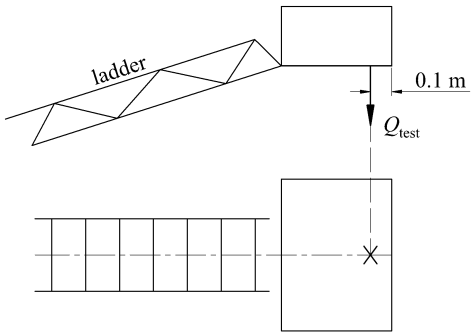

Figure 7. The applicable position of Q_{tests} and Q_{testd}

Table 6. Load combinations in the third case

No.	Combination	Load combination formula	φ (°)		Factor value [20, 21]
			0	75	
1	Comb. 28	$\beta\left[\beta_1\cdot G+\beta_4\left(Q_{tests}+F_r+F_t\right)\right]$	×	×	
2	Comb. 29	$\beta\left[\beta_1\cdot G+\beta_4\left(Q_{testd}+F_r+F_t\right)+\beta_5\cdot F_l+F_{wp}\right]$	×	×	
3	Comb. 30	$\beta\left[\beta_1\cdot G+\beta_4\left(Q_{testd}+F_r+F_t\right)+\beta_5\cdot F_s+F_{wp}\right]$	×	×	
4	Comb. 31	$\beta\left[\beta_1\cdot G+\beta_4\left(Q_{testd}+F_r+F_t\right)+\beta_5\cdot F_l+F_{wf}\right]$		×	$\beta = 1.22$
5	Comb. 32	$\beta\left[\beta_1\cdot G+\beta_4\left(Q_{testd}+F_r+F_t\right)+\beta_5\cdot F_s+F_{wf}\right]$		×	$\beta_1 = 1$ $\beta_4 = 1$
6	Comb. 33	$\beta\left[\beta_1\cdot G+\beta_4\left(Q_{testd}+F_r+F_t\right)+\beta_5\cdot F_l+F_{wb}\right]$	×		$\beta_5 = 1.2$
7	Comb. 34	$\beta\left[\beta_1\cdot G+\beta_4\left(Q_{testd}+F_r+F_t\right)+\beta_5\cdot F_s+F_{wb}\right]$	×		
8	Comb. 35	$G+\left(1,5\cdot Q_p+Q_a+F_r+F_t\right)$		×	
9	Comb. 36	$G+\left(F_r+F_t\right)$		×	

4. Regulatory tests

The stress ratio of an element which has a tension force, and a bending moment is defined as follows:

$$f = \frac{\sigma_t}{[\sigma_t]} + \frac{\sigma_b}{[\sigma_b]} \tag{9}$$

where σ_t is the tension stress produced by axial tension loads (N/mm^2); σ_b is the maximum bending stress produced by applied bending moment (N/mm^2); $[\sigma_t]$ is the allowable stress for tensioned elements (N/mm^2) and $[\sigma_b]$ is the allowable bending stress for members subjected to bending only (N/mm^2).

The stress ratio of the element bore a combined load inclusive shear load, compression load, and bending moment is determined as follows:

$$f = -\left[\frac{\sigma_c}{[\sigma_c]} + \frac{\sigma_b}{[\sigma_b]} + \left(\frac{\tau}{[\tau]}\right)^2\right] \tag{10}$$

where σ_c is the compressive stress produced by axial compressive loads (N/mm^2); $[\sigma_c]$ is the allowable compressive stress for member subjected to compression only (N/mm^2); τ is the shear stress caused by torsion or transverse shear loads (N/mm^2) and $[\tau]$ is the allowable shear stress for member subjected only to torsion or shear (N/mm^2).

The stress ratio must satisfy the condition in (11) [23]:

$$|f| \leq 1 \tag{11}$$

The impact of the tension load of the steel wire ropes will be thoroughly considered and primarily evaluated through their correlative responses.

According to [15], the difference of the displacement at the top ladder calculated from the combinations must be less than 100 mm.

5. Effect of steel rope tension on the structure

Investigating stress ratio f in 34 combinations as shown in Tables 4–6 corresponding to 8 levels of F_{ri} $(i = 1, 2, 3)$ as shown in Table 1, the elements that have large values of f are pointed out in Fig. 8.

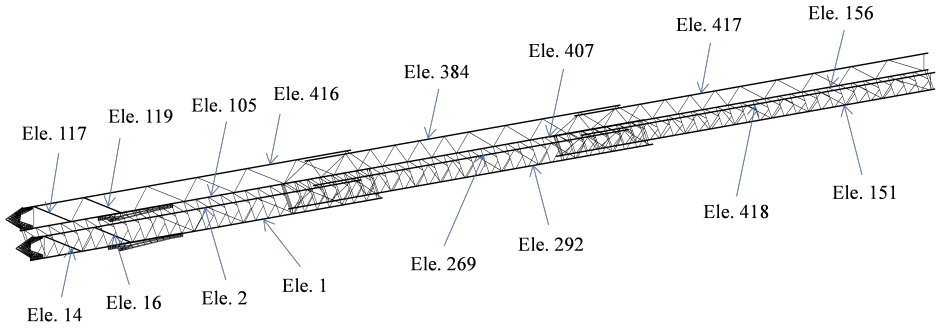

Figure 8. Elements having large values of f

They include the diagonal web elements (Eles. 14, 117) and (Eles. 16, 119); the handrails (Eles. 417, 418), (Eles. 384, 169) and (Eles. 416, 2); and the rails (Eles. 156, 151), (Eles. 407, 292) and (Eles. 105 and 1). Their maximum values of $f$are presented as in Fig. 9. Here, the negative sign only indicates the compressed state.

The maximum values of the stress ratio in two diagonal web elements 14 and 117 increases and they still satisfy the stress condition. Without these elements, the ratios of the others which have the high stress ratio are reduced in both positions. During the increasing process of the values of k_{ri} $(i = 1, 2, 3)$ the maximum stress ratios steadily change. In element 151, the maximum ratio can appear in two combinations and at two cross sections, except that it appears at the fixed positions and the fixed combinations. At $\varphi = 0°$, the highest stress occurs in the ladder structure. At $\varphi = 75°$, the maximum stress of the elements is significantly smaller. The maximum stress change in this case when changing load combinations is complex.

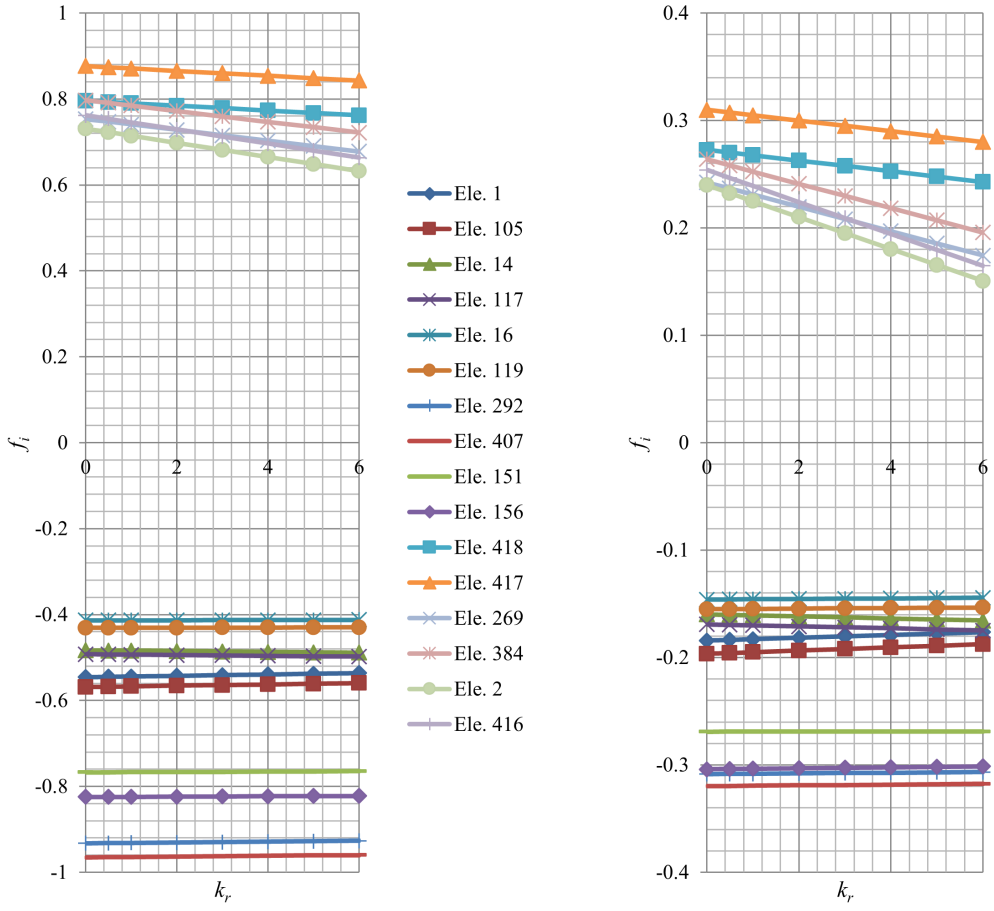

(a) $\varphi = 0°$ (b) $\varphi = 75°$

Figure 9. Stress ratios of the considered elements

For the handrails where the steel wire ropes are added into, without the short cantilever parts (76 mm, 102 mm, and 114 mm correspond to sections 1, 2, and 3) at their ends and the compressed zones with low compression forces, the others are still tensioned and satisfy the stress condition in all

load combinations.

In the state when the truck does not work, the sections are stacked. Assuming the stress in the handrails caused by their gravity and the cage is negligible. The effect of the diagonal web elements on the stability of the handrail in the horizontal plane which contains it is also assumed to be negligible. The tension load of the ropes is limited by the limited compressive force of the handrail. It is given by

$$F_{\text{lim}} = \frac{\pi^2 E I_{\text{min}}}{L_e^2} \tag{12}$$

where π is Archimedes' constant; E is Young's modulus (N/m^2); L_e is the calculation length of elements (m); and I_{min} is the minimum value of area moment of inertia (m^4).

With the known parameters, the compressive forces in the handrails of the ladder sections 1, 2 and 3 are 1307 N, 6272 N, and 11097 N, respectively.

The pre-tensioned loads must be smaller than the above forces. It means that the ropes should be stretched to the level 4 (Table 1). In case, the tension loads wanting to become greater, they can be increased during or after the extending process.

The static displacement caused by the rated load and the difference between the displacements at the ladder top of combinations 35 and 36 are shown in Fig. 10(a) and Fig. 10(b), respectively. Their values also significantly reduce. They are inversely proportional to the values of k_{ri}. Their reduction rates are summarized in Table 7.

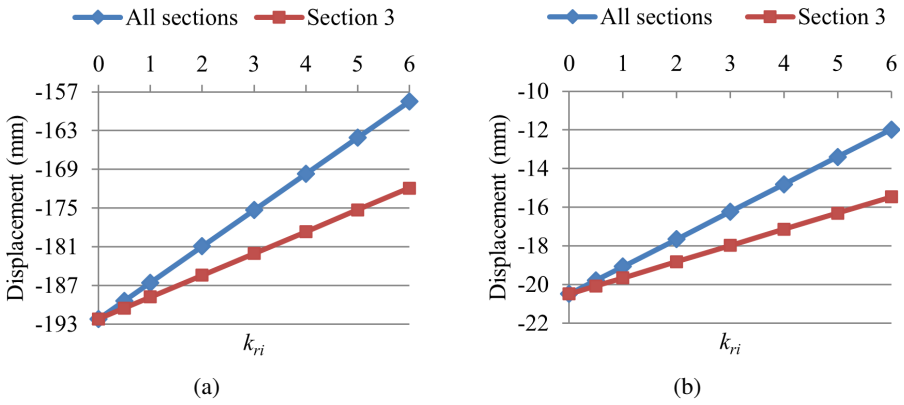

Figure 10. The static displacement (a) caused by Q and the difference between the displacements (b) at the ladder top of combinations 35 and 36

Table 7. Displacement reduction rates in case ropes added in the ladder

k_{ri}		0.5	1	2	3	4	5	6
Displacement in Fig. 10(a)	All sec.	1.5%	2.9%	5.8%	8.8%	11.7%	14.6%	17.5%
	Sec. 3	0.9%	1.8%	3.5%	5.3%	7.0%	8.8%	10.5%
Displacement in Fig. 10(b)	All sec.	3.5%	6.9%	13.9%	20.8%	27.7%	34.6%	41.6%
	Sec. 3	2.0%	4.1%	8.2%	12.3%	16.4%	20.4%	24.5%

The static displacement reduction can reach 10.5% or 17.5% depending on the ropes being stretched at section 3 or all sections. Similarly, in the displacement comparison condition prescribed in [15], the maximum reduction is 24.5% and 41.6%, corresponding to those two rope pulling options.

6. Conclusions

To ensure that the turntable ladder still normally works, testing the impact of the steel wire rope added into the handrails through 36 load combinations specified by the relevant standards is carried out.

The impact of the tension load in this investigation at the defined level has the effect of enhancing the load capacity of the rails and the handrails. It also creates a negative effect on some elements, e.g., elements 14 and 117. They are two of the elements belonging to the maximum stress ratio group. However, the increase is not large, and the ladder structure remains within the safe range.

The static displacement at the ladder top significantly reduces. The decrease gets larger as the tension load increases.

The value of the pre-tension loads should not exceed level 4 (in Table 1) as the turntable ladder has not worked. In case of necessity, the load can be increased in or after the extending process.

The tension load of the ropes in section 3 has the most effect. Moreover, the possibility of increasing its value is more positive.

To achieve greater performance of the load, it should be able to be adjusted as needed. That means having to establish an appropriate rope tension unit.

References

[1] Tremblay, J. (2013). *Tower Rescue Emergency Module*. US Patent, No. US 2013/0206505 A1, USA.

[2] Renton, J. E., Nott, P. T. M. (2009). *Personnal Height Resuce Apparatus*. US Patent, No. US 2009/0173578 A1, USA.

[3] Giang, D. T., Tinh, N. V., Dang, N. T. T. (2021). Research on designing the individual rescue winch. *Journal of Science and Technology in Civil Engineering (STCE) - HUCE*, 15(1V):123–133. (in Vietnamese).

[4] Duong, T., Nguyen, V. T., Nguyen, T. D. (2021). Optimizing the weight of the two-level gear train in the personal rescue winch. *Archive of Mechanical Engineering*, 68.

[5] Burman, M. J., Goodson, S. E., Aiken, J. D. (2009). *Telescopic aerial ladders; components; and methods*. US Patent, No. US 2009/0101436 A1, USA.

[6] Arps, E. J. (1956). *Aerial extension ladder*. US Patent, No. US 2732992, USA.

[7] Zimmert, N., Kharitonov, A., Sawodny, O. (2008). A new Control Strategy for Trajectory Tracking of Fire–Rescue Turntable Ladders. *IFAC Proceedings Volumes*, 41(2):869–874.

[8] Zimmert, N., Pertsch, A., Sawodny, O. (2012). 2-DOF Control of a Fire-Rescue Turntable Ladder. *IEEE Transactions on Control Systems Technology*, 20(2):438–452.

[9] Pertsch, A., Sawodny, O. (2016). Modelling and control of coupled bending and torsional vibrations of an articulated aerial ladder. *Mechatronics*, 33:34–48.

[10] Nguyen, V. T., Schmidt, T., Leonhardt, T. (2019). Effect of pre-tensioned loads to vibration at the ladder tip in raising and lowering processes on a turntable ladder. *Journal of Mechanical Science and Technology*, 33(5):2003–2010.

[11] Nguyen, V. T., Schmidt, T., Leonhardt, T. (2021). A new active vibration control method on a ladder of turntable ladders. *Journal of Mechanical Science and Technology*, 35(6):2337–2345.

[12] Duong, T. G. (2017). Research on fundamental calculation of tower cranes examining into the elastic deflections of tower body. *Journal of Science and Technology in Civil Engineering (STCE) - HUCE*, 11 (4):139–144. (in Vietnamese).

[13] Nguyen, V. T., Nguyen, K. A., Nguyen, V. L. (2019). An improvement of a hydraulic self-climbing formwork. *Archive of Mechanical Engineering*, 66(4).
[14] Horváth, P., Hajdu, F., Kuti, R. (2020). Investigation of swings caused by sudden wind loads during operation of an aerial ladder. *FME Transactions*, 48(2):351–356.
[15] BS EN 14043:2014. *High Rise Aerial Appliances for Fire Service Use - Turntable Ladders with Combined Movements - Safety and Performance Requirements and Test Methods*. British Standards Institution, UK.
[16] FEM 1.001 (1998). *Rules for the Design of Hoisting Appliances*. European Material Handling Federation, Brussels, Belgium.
[17] DIN EN 1777:2010-06 (2010). *Hydraulic Platforms for Fire Fighting and Rescue Services - Safety Requirements and Testing*. Brussels, Belgium.
[18] BS EN 280:2013+A1:2015. *Mobile Elevating Work Platforms - Design Calculations - Stability Criteria - Construction - Safety - Examinations and Tests*. British Standard, UK.
[19] ISO 4302:2016. *Cranes - Wind load assessment*. Geneva, Switzerland.
[20] ISO 8686-1:2012. *Cranes - Design principles for loads and load combinations - Part 1: General*. Geneva, Switzerland.
[21] ISO 8686-2:2018. *Cranes - Design principles for loads and load combinations - Part 2: Mobile cranes*. Geneva, Switzerland.
[22] ISO 4310:2009. *Cranes - Test code and procedures*. Geneva, Switzerland.
[23] 24 CFR 200-Subpart S (1968). *Aluminum Construction Manual- Specifications for Aluminium Structures*. The Aluminum Association, USA.